

# Comprehensive Physical Model for the Contrasting Seismogenic Behaviours of Injection Wells in the Kiskatinaw Seismic Monitoring and Mitigation Area, Northeastern British Columbia (NTS 093P, 094A)

**B. Wang, School of Earth and Ocean Sciences, University of Victoria, Victoria, British Columbia  
beiwang@uvic.ca**

**H. Kao, Natural Resources Canada, Geological Survey of Canada–Pacific, Sidney, British Columbia**

**H. Yu, Natural Resources Canada, Geological Survey of Canada–Pacific, Sidney, British Columbia**

**R. Visser, Natural Resources Canada, Geological Survey of Canada–Pacific, Sidney, British Columbia**

**S. Venables, British Columbia Oil and Gas Commission, Victoria, British Columbia**

---

Wang, B., Kao, H., Yu, H., Visser, R. and Venables, S. (2022): Comprehensive physical model for the contrasting seismogenic behaviours of injection wells in the Kiskatinaw Seismic Monitoring and Mitigation Area, northeastern British Columbia (NTS 093P, 094A); *in* Geoscience BC Summary of Activities 2021: Energy and Water, Geoscience BC, Report 2022-02, p. 35–48.

## Introduction

Induced earthquakes are defined as events caused by anthropogenic activities and their occurrence can be traced back over five decades (Healy et al., 1968; Raleigh et al., 1976). During the past ten years, subsurface fluid injection has drawn increasing attention due to its association with a dramatic increase in regional/local seismicity; for example, the number of earthquakes of magnitude ( $M_w$ ) >3 increased by a factor of 10 in the central United States. Most of these events have been attributed to wastewater-disposal (WD) operations that are often associated with high injection rates and a large amount of cumulative volume (Ellsworth, 2013; Keranen and Weingarten, 2018). Comparably, hydraulic fracturing (HF) stimulations can also trigger  $\geq M_w$  4 earthquakes, and many cases have been documented in areas such as the Western Canada Sedimentary Basin (WCSB) and southwestern China (e.g., Atkinson et al., 2016; Bao and Eaton, 2016; Schultz et al., 2018; Lei et al., 2019; Wang et al., 2020; Yu et al., 2020).

Progress has been made to characterize the various controlling factors of the HF-related injection-induced earthquakes (IIEs) in the WCSB. For example, Schultz and Eaton (2018) suggested that IIEs preferentially locate within regions with overpressured formations, whereas Schultz et al. (2016) and Galloway et al. (2018) found that specific geological conditions, such as the reef margins and fault-related karst features, tend to correlate with more IIEs due to their ability to guide fluid flow to the faults. Similarly, Peña Castro et al. (2020) and Wang et al. (2020) proposed that several of the largest IIEs in western Canada

have occurred on pre-existing faults, with possible direct connection to highly permeable conduit structures. Schultz et al. (2018) further delineated a linear relationship between the cumulative injection volume of a single HF pad and the number of HF-related IIEs. Many studies also suggested that in situ regional stress could be another important factor facilitating seismic slip on a fault (e.g., Zoback and Lund Snee, 2018; Shen et al., 2019). On a regional scale, Kao et al. (2018) pointed out that the tectonic-strain rate plays a key role in controlling the spatial distribution of IIEs in the WCSB.

These innovative breakthroughs provided a first-order understanding of the seismogenic factors associated with IIEs in the WCSB. However, comprehensive investigations to evaluate the relative significance of each of these factors are hindered by the lack of a high-quality catalogue of IIEs and the limited access to well-operation databases. In addition to delineating possible controlling factors of IIEs in western Canada, two key questions related to their causal mechanisms also need to be considered. The first relates to the reason why the seismic response to comparable injection activities within the same shale play varies significantly. An interesting example is the Duvernay play in Alberta, where the Kaybob region is more seismogenic than the Willesden Green or Edson regions (Schultz et al., 2018). The other is concerned with how to forecast the corresponding seismogenic behaviour when multiple formations are targeted by the same HF pad. A typical example is the Kiskatinaw Seismic Monitoring and Mitigation Area (KSMMA) in northeastern British Columbia (BC), where the gas-bearing stratigraphy of the Montney Formation can be subdivided, from top to bottom, into the Upper Montney (UM), upper Middle Montney (UMM), lower Middle Montney (LMM) and Lower Montney (LM) members (Figure 1;

---

*This publication is also available, free of charge, as colour digital files in Adobe Acrobat® PDF format from the Geoscience BC website: <http://geosciencebc.com/updates/summary-of-activities/>.*

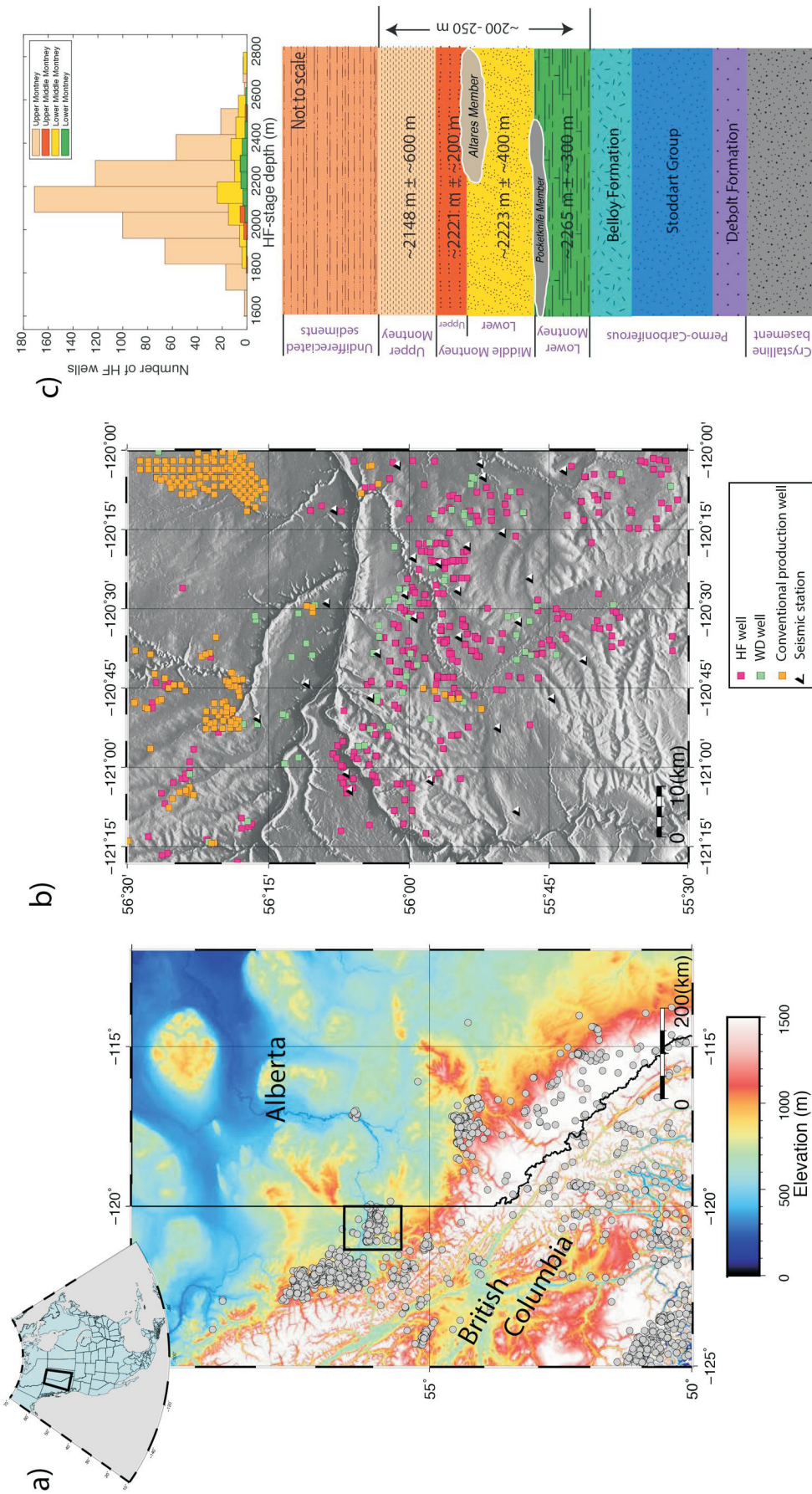


**Figure 1.** Spatial distribution of earthquakes and injection wells in western Canada. **a)** Grey circles mark epicentres of magnitude 3 or greater seismicity in northeastern British Columbia and western Alberta between 2011 and 2020, as reported by Natural Resources Canada. The black rectangle marks the study area in the Kiskatinaw Seismic Monitoring and Mitigation Area in northeastern British Columbia. **b)** Hydraulically fractured production wells (HF) and wastewater-disposal wells (WD), conventional oil-and-gas production wells and seismic stations in the study area. **c)** Top panel shows the number of HF wells targeting different Montney Formation members as a function of depth; bottom panel shows a stratigraphic column of the Montney Formation and the underlying Permo-Carboniferous formations.

Davies et al., 2018). The HF operations targeting these members offer a natural laboratory in which to differentiate the possible seismic response within different stratigraphic units.

The seismic-station coverage in northeastern BC has been systematically improved since 2013 (Figure 1). Over the years, the newly established stations have lowered the regional earthquake-detection threshold by 1 to 2 units of magnitude (Babaie Mahani et al., 2016; Babaie Mahani, 2021) and thus provide a unique opportunity to enhance the existing earthquake catalogue (Visser et al., 2017, 2020) as well as to investigate, at an unprecedented resolution, the detailed spatiotemporal distribution of IIEs relative to potential influencing factors. In this study, a series of Monte Carlo tests and detailed statistical analysis based on an enhanced earthquake catalogue were used to determine the relative significance of physical factors that control the local seismogenic pattern of IIEs. A comprehensive model was developed, using injection type, regional structural geology and stratigraphic setting as the top three factors explaining observations from the study. Initial observations presumably indicate that injections, even at the same geographic location, can have very different IIE responses, depending on the target's stratigraphic setting. This finding will help bridge the gap in understanding how anthropogenic/hydrogeologic/stratigraphic factors impact the occurrence of IIEs and lead to substantial progress in effectively mitigating injection-related seismic hazard.

## Data and Methods

The fluid injection parameters from completion reports in the BC Oil and Gas Commission database (BC Oil and Gas Commission, 2021) were compiled. Wastewater-disposal injection is usually a continuous process lasting for months or years, in contrast to a HF stage that is often finished within a few hours. There is also a big difference in the injection rate ( $\sim 0.5 \text{ m}^3/\text{min}$  in the case of WD injections vs.  $\sim 10 \text{ m}^3/\text{min}$  in that of HF injections). In this study, the WD- and HF-injection operations in the stratigraphic unit are quantified by month and stage, respectively, based on the technical/completion reports submitted to the regulator by local operators. In total, 20 293 HF stages were undertaken at 778 horizontal wells and 58 WD-injection wells were active for 1151 months. Detailed information on the stratigraphic setting of all injection wells is retrieved from the BC Oil and Gas Commission (2021) database.

The waveform data used has been retrieved from broadband seismic stations belonging to three local and regional seismograph networks (network codes XL, 1E and PQ, operating at a digitization rate of 100 samples/s). The first step consisted in deploying the sophisticated earthquake-location method, referred to as 'source-scanning based on navigated automatic phase-picking' (Tan et al., 2019), to detect

and locate events within the study area that occurred between January 1, 2017 and December 31, 2018. To minimize errors resulting from inaccurate travel times, the 1-D velocity model developed specifically for the KSMMA area by Babaie Mahani et al. (2020) was adopted. About 250 times more events have been detected and located (10 693 events in total; Figure 2a) using the method outlined in this study, compared to the number reported in the standard Natural Resources Canada (NRCAN) earthquake catalogue (Natural Resources Canada, 2021), which is mainly based on visual inspection of seismic phases recorded by much fewer stations.

Next, the newly developed depth-scanning algorithm (DSA; Yuan et al., 2020) is used to refine the focal depth of earthquakes of  $M_w$  2.5 or greater recorded in the enhanced catalogue. The DSA improves the focal-depth accuracy by incorporating the travel-time constraint from depth phases recorded at local and regional distances. The scanning range of focal depth is set at 1 to 35 km and the scanning process consists of three major steps: firstly, the waveforms of all possible depth phases are constructed from the direct P and S phases; secondly, the synthetic depth-phase waveforms are used as templates to scan the observed seismograms for any segments with high waveform similarity; lastly, the depth corresponding to the largest number of depth-phase matches and minimum accumulated travel-time residual is deemed the final solution.

Using the enhanced earthquake catalogue and compiled fluid-injection data, a Monte Carlo test is conducted, following the method presented in Schultz et al. (2016), to verify whether IIEs are statistically correlated with injection activities. Based on the naive assumption that all epicentres are randomly distributed, 10 000 synthetic catalogues (each with the same number of events as the real catalogue) are created. For each synthetic catalogue, the average distance between earthquake epicentre and the nearest injection activity is calculated. These 10 000 event-to-well averaged-distance values from the synthetic catalogues are then compared with the actual distances derived from the real catalogue and injection data.

Finally, by deploying a spatiotemporal correlation filter (STCF), IIEs are associated with corresponding HF stages to determine the role of the stratigraphic setting, as was done in a prior study (Schultz et al., 2018). As a prerequisite, the earthquake must have occurred within a certain time window after the stimulation stage. Once this temporal criterion is satisfied, the earthquake is assigned to the nearest HF stage, so long as the pair also satisfies the spatial criterion.

## Results

In this section, the physical factors that control the pattern of IIEs in the KSMMA are systematically delineated. By

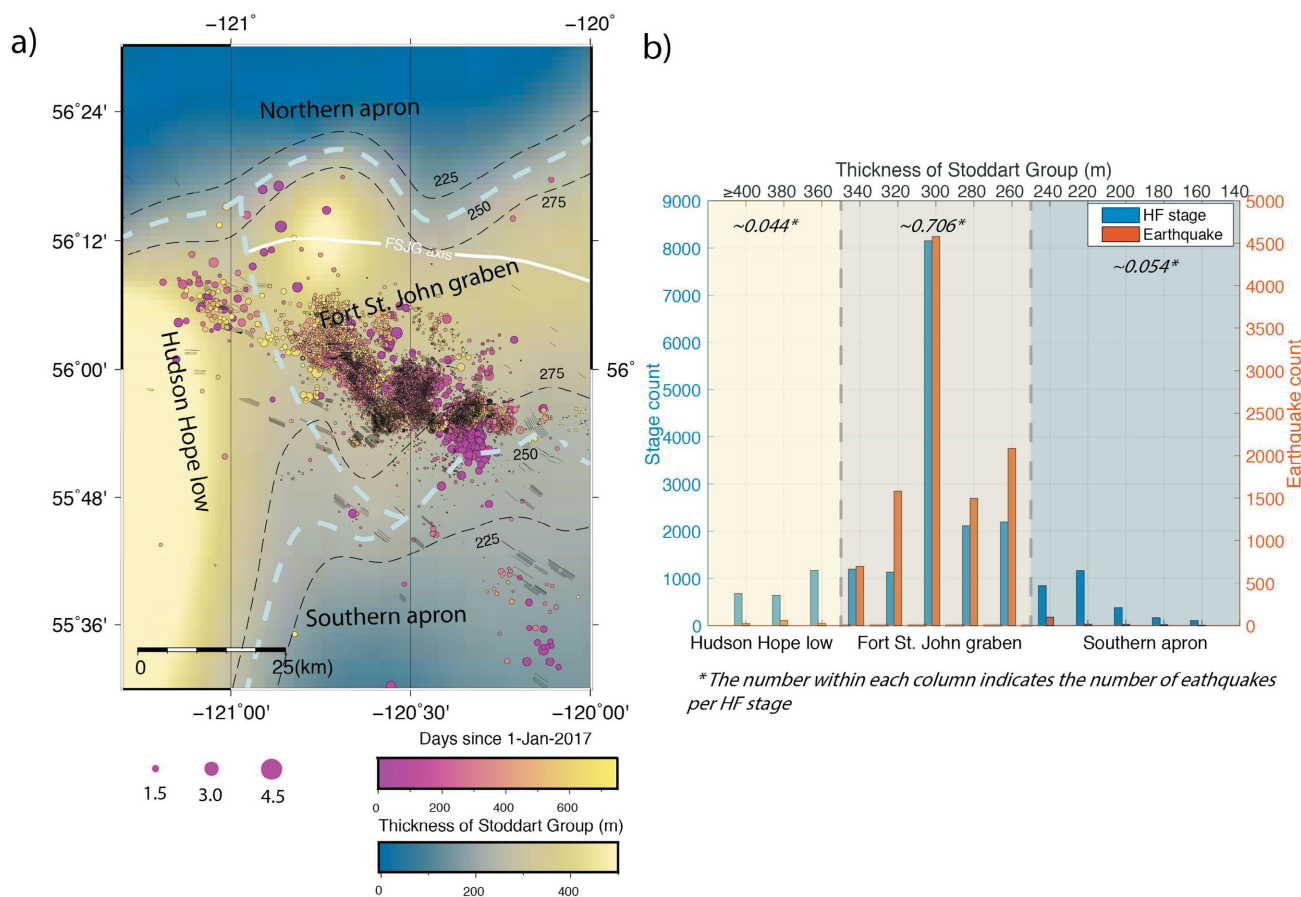


**Figure 2.** Major geological structures and seismic pattern in the study area, northeastern British Columbia. **a)** Spatiotemporal distribution of injection-induced earthquakes with respect to the regional structural geology. Thick dashed lines represent the inferred boundaries of different tectonic elements based on the thickness (thin dashed lines) of the Stoddart Group (SG). The inferred boundary between the Fort St. John graben (FSJG) and the deeper Hudson Hope low to the west is shown as well as the FSJG axis indicated by the white line (adapted from O’Connell, 1994). **b)** Number of hydraulic-fracturing stages and earthquakes corresponding to different SG thicknesses. Note that the SG thickness of each earthquake is approximated with the measurement corresponding to the closest hydraulic-fracturing (HF) well.

comparing the level of seismicity of comparable injection activities, an attempt is made to determine the relative significance of the recognized factors.

### Most Influential Factor: Injection Type

As shown in Figure 3, the Monte Carlo-simulation results suggest that the randomly generated synthetic catalogues all present significantly greater event-to-well distances when compared to the real earthquake catalogue (~10 km vs. ~1 km). The distance difference becomes even greater once a temporal constraint of no longer than five days is imposed on the triggering delay (~35 km vs. ~7 km). Since none of the 10 000 synthetic catalogues yields an averaged event-to-well distance comparable to the observed value, the probability of earthquakes being randomly distributed in the study area must be  $<10^{-4}$ . This result suggests that the association proposed between earthquake occurrence and injection operations is statistically significant.

The average distance between individual catalogued earthquakes and the nearest HF and WD wells is then calculated,

following the approach used in Schultz et al. (2018). The average distance from an earthquake epicentre to the closest WD operation has been found to be approximately four times the distance associated with the closest HF stage (~4 km vs. ~1 km; Figure 3c), which suggests that HF activities might play a more significant role in inducing these events.

### Secondary Factor: Regional Structural Geology

In the study area, the predominant geological structure is the Dawson Creek graben complex (DCGC), consisting of the core Fort St. John graben (FSJG), the western zone of greater subsidence (i.e., the Hudson Hope low [HHL]), the northern and southern sediment aprons, and the smaller satellite grabens to the east (Barclay et al., 1990; O’Connell, 1994). The structural development of the DCGC is closely linked to the deposition of the Stoddart Group (SG) and the thin, overlying Belloy Formation (Barclay et al., 1990). Barclay et al. (1990) used the thickness of the SG as a proxy to estimate the boundary of the FSJG, which is an asymmetric structure with a gently sloping, but less constrained,

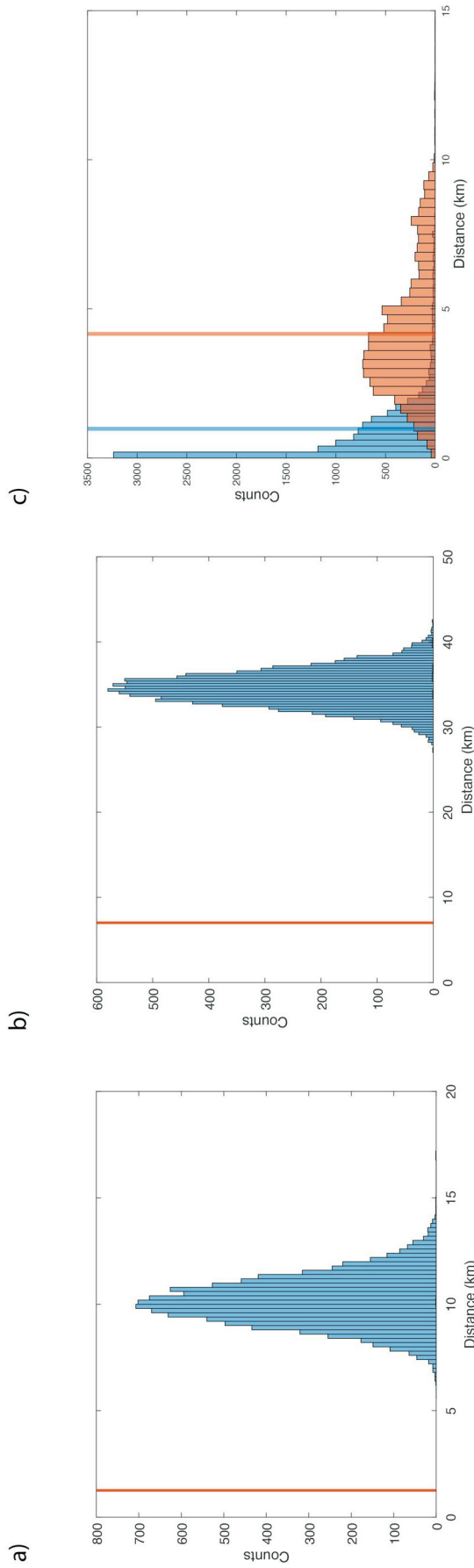


**Figure 3.** Results of Monte Carlo tests used to examine whether the seismicity observed in the study area, northeastern British Columbia, is correlated with injection operations. **a)** Assuming that earthquake epicentres are randomly distributed, the histogram shows the distribution of the average distance between an epicentre and the nearest injection well from a population of 104 synthetically generated catalogues. This experiment is done without imposing a time constraint. The solid vertical line represents the average distance between an epicentre and the nearest injection well, derived from an enhanced earthquake catalogue (using a total of 10 693 events). **b)** Similar to a), but with a five day time constraint to correlate the earthquake to the nearest injection well. **c)** Distribution of the distance between an earthquake epicentre and the nearest hydraulic fracturing (blue bars) or wastewater-disposal (red bars) well. The two vertical lines represent the average values.

southern apron. Conventionally, different thickness contours of the SG are used to define the northern (150–200 m) and southern (270–300 m) edges of the FSJG (Figure 2a). However, in this study, a more consistent approach is taken and the boundary between the FSJG and the surrounding aprons is set at the SG-thickness contour of 250 m (Figure 2a).

The number of earthquakes and HF stages within the areas of FSJG, HHL and the southern apron (the number of HF wells in the northern apron is insufficient) was counted. As shown in Figure 2b, the level of seismicity is the highest within the FSJG area (corresponding to a SG thickness between 250 and 350 m), whereas the number of earthquakes is almost negligible in the HHL and southern apron areas. In total, 10 439, 110 and 144 events were observed for the FSJG, HHL and southern apron areas, respectively, whereas the corresponding number of HF stages performed in these three areas were recorded as 14 778, 2488 and 2642, respectively. On average, the ratio between the number of earthquakes and HF stages is  $\sim 0.706$  in the FSJG area, but only  $\sim 0.044$  and  $\sim 0.054$  in the areas of the HHL and southern apron. These results suggest that HF injections in the FSJG area have a much greater likelihood of inducing an earthquake.

The next step consists in examining whether the drastically different levels of local seismicity can be explained as the result of the injection of different cumulative volumes of fluids. It turns out that the cumulative injected volume is approximately linearly correlated with the cumulative

number of HF stages (Figure 4). Consequently, the total volume of HF injections in the FSJG area is approximately 5.9 times higher than that in the HHL area and  $\sim 5.6$  times higher than that in the southern apron. The number of earthquakes per one million cubic metres of injected volume is  $\sim 1413$  for the FSJG area, which is  $\sim 15$  times higher than the number of events in the HHL ( $\sim 88$ ) and southern apron ( $\sim 107$ ) areas. Therefore, the difference between injection volumes cannot fully account for the extreme variations of local seismicity in the three subareas; these ratios again underscore the significance of the area’s geological structures.

### Third Factor: Stratigraphic Setting

In the KSMMA, the majority of HF stimulations aim at the UM, followed by the LMM, and only a very small number of HF wells target the UMM and LM (Figure 1c). The depth of each Montney member can vary from one location to another, ranging from  $\sim 1.5$  to  $\sim 2.5$  km below the surface, as inferred from HF completion reports. Overall, the total thickness of the Montney Formation is  $\sim 100$ – $250$  m. The seismic response to injections within the different members (or depths) remains unclear.

Figure 5 shows the results of a STCF analysis using time and distance thresholds of 3 days and 3 km, respectively. While the number of HF stages targeting the LMM is only  $\sim 1/5$  of that targeting the UM, the number of IIEs associated with the LMM HF stimulations is much higher (Figure 5b). Furthermore, a *p*-value was calculated to test the validity of a null hypothesis proposing that HF stages tar-

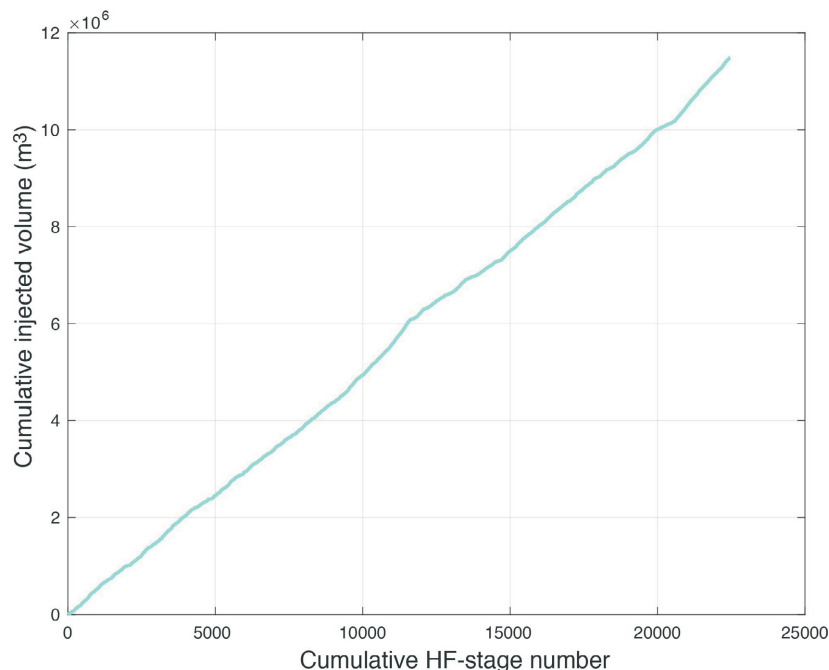


**Figure 4.** The relationship between the number of cumulative hydraulic fracturing (HF) stages and the cumulative injected volumes within the Kiskatinaw Seismic Monitoring and Mitigation Area, northeastern British Columbia, for 2017 and 2018.

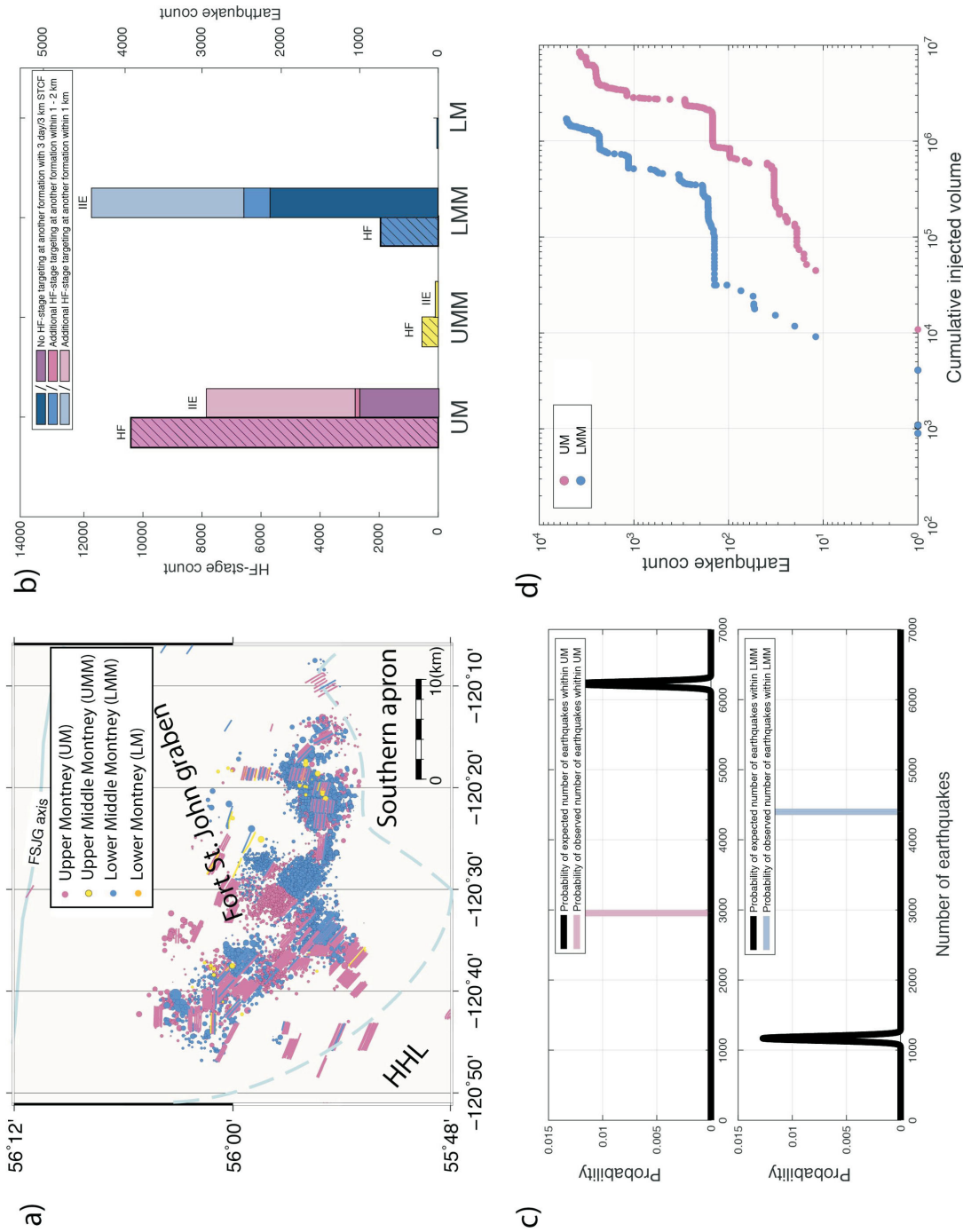


**Figure 5.** Statistical results after applying a 3 day and 3 km spatiotemporal correlation filter (STCF). **a)** Spatial distribution of epicentres (circles) and surface projections of horizontal hydraulic-fracturing (HF) wells (thin lines) associated with injections into different Montney Formation members, northeastern British Columbia. **b)** Histograms showing the number of HF stages and earthquakes associated with each Montney member. The level of confidence in the correlation between HF stage and injection-induced earthquake (IIE) is reflected in the tone of the colour (darker means higher confidence level). **c)** Probability as a function of the designated number of earthquakes associated with HF (thick black line) in the UM (top panel) and LMM (bottom panel), assuming that earthquakes can be equally triggered by HF stages, regardless of the targeted member. Coloured vertical lines mark the observed number of earthquakes. **d)** Number of earthquakes as a function of the cumulative injected volume for the UM and LMM. Abbreviations: FSJG, Fort St. John graben; HHL, Hudson Hope low; LM, Lower Montney; LMM, Lower Middle Montney; UM, Upper Montney; UMM, Upper Middle Montney.

getting the UM and LMM have the same earthquake-triggering capacity. The number of earthquakes predicted by this hypothesis (solid black lines, Figure 5c) is completely inconsistent with observations made during this study (pink and blue lines, Figure 5c), which suggests that the null hypothesis can be statistically rejected.

Finally, to quantitatively characterize the different seismic responses of the UM and LMM, the volumes used in individual HF stages and the number of IIEs for the two members were compiled separately, and the result is shown in Figure 5d. It is interesting to note that the two lines are similar except that the UM has approximately one time more cumulative volume, given the same IIE count. This difference suggests that the likelihood of IIEs being triggered in the LMM is probably one time greater than that in the UM.

### Other Operational Factors

In addition to the injected volume, other operational parameters that could contribute to the discrepancy in IIE-triggering capacity in the three areas were also investigated, including breakdown pressure, injection rate, shut-in pressure and average treating pressure. All these operational parameters appear to have comparable values without following the IIE-distribution pattern (Figure 6). Therefore, the difference is not large enough to justify the dramatic difference noted in the observed seismic pattern.

### A Physical Model to Interpret the Contrasting Seismogenic Behaviours

After delineating the controlling factors associated with deep fluid injection, a comprehensive model was developed to interpret the findings. Figure 7 is a schematic diagram summarizing this physical model; three factors are considered in the model. The first, and most important, controlling factor is the injection type; as shown in Figure 3, and suggested by the results of the Monte Carlo tests, the vast majority of IIEs in the KSMMA are associated with HF injections (~80%, given a 3 day and 3 km STCF criterion). The second important controlling factor is the regional structural geology; specifically, HF-related IIEs are more likely to occur if stimulations are performed in the FSJG area than in the neighbouring HHL and southern apron areas. Lastly, the third controlling factor is the stratigraphic setting; once inside the FSJG area, HF stages targeting the LMM are found to statistically cause more IIEs than those targeting other formations, even though the corresponding cumulative injected volume is ~5 times lower.

The fact that HF stimulations in the study area are associated with many more IIEs than WD injections did not come as a surprise, since a similar conclusion had been reported in previous studies (Atkinson et al., 2016; Schultz and Eaton, 2018; Yu et al., 2020; Wang et al., 2021). However, care should be taken when interpreting this observation. A

direct communication with the regulator confirms that all WD-well locations in northeastern BC were carefully selected to minimize the chance of causing IIEs. Specifically, they avoid any known fault structures and target reservoirs that are less communicable to surrounding formations with confining layers. Thus, the contrasting seismic responses to HF and WD may be, at least in part, a consequence of the industry's own mitigation practice in the KSMMA.

The higher number of HF-related IIEs in the FSJG area than in the surrounding HHL and apron areas may be explained by the presence of unique geological characteristics. The FSJG has been intensely segmented and faulted into blocks during tectonic subsidence (Barclay et al., 1990). A recent study based on the spatiotemporal distribution of HF-related IIEs and high-resolution 3-D seismic images near Fort St. John reveals multiple buried thrust faults extending from the basement up to the Montney Formation and a pervasive system of transverse structures (Riazi and Eaton, 2020). These faults could act as potential pathways, along which aseismic pore-pressure diffusion can migrate farther, thus increasing the possibility of causing more IIEs in the vicinity (e.g., Ryan Schultz et al., 2016; Lei et al., 2017; Galloway et al., 2018; Eyre et al., 2019; Peña Castro et al., 2020; Yu et al., 2020; Wang et al., 2021). Moreover, one of the largest fault systems in the region, the Gordondale fault, runs subparallel to the axis of the FSJG and extends eastward into central Alberta (Eaton et al., 1999); it could also contribute to the higher potential of IIEs in the FSJG area.

The more active seismogenic behaviour of the LMM, as compared to that of the UM, could be related to its greater depth and unique stratigraphic setting. Many previous studies have suggested that larger IIE sequences tend to nucleate on pre-existing faults, located in the deeper crystalline basement, that are reactivated by fluid injections (e.g., Bao and Eaton, 2016; Schultz et al., 2016; Lei et al., 2017; Skoumal et al., 2018; Lei et al., 2019; Riazi and Eaton, 2020; Wang et al., 2020). In the study area, the recalibrated focal depths of the two largest IIEs ( $M_w$  4.5 on November 30, 2018 and  $M_w$  3.3 on November 30, 2018) are also located deeper than the Montney Formation at ~2.6 and ~3.9 km, respectively, most likely in the crystalline basement. More importantly, there are two newly recognized groups of bioclastic beds, known as the Altares Member (AM) and Pocketknife Member (PKM), intercepting and interfingering with the LMM at the top and bottom sections, respectively (Figures 1c, 7c; Zonneveld and Moslow, 2018). Both members have a distinctly low total organic carbon (TOC) content and high proportion of recrystallized skeletal calcite from shell materials. As calcite-rich fault-gouge joint surfaces generally have higher shear strength than those coated with clayey material (Ikari et al., 2013; Verberne et al., 2014), it is conceivable that deformation caused by fluid injection within the LMM, interfingering with the AM and PKM, is more likely to manifest itself as

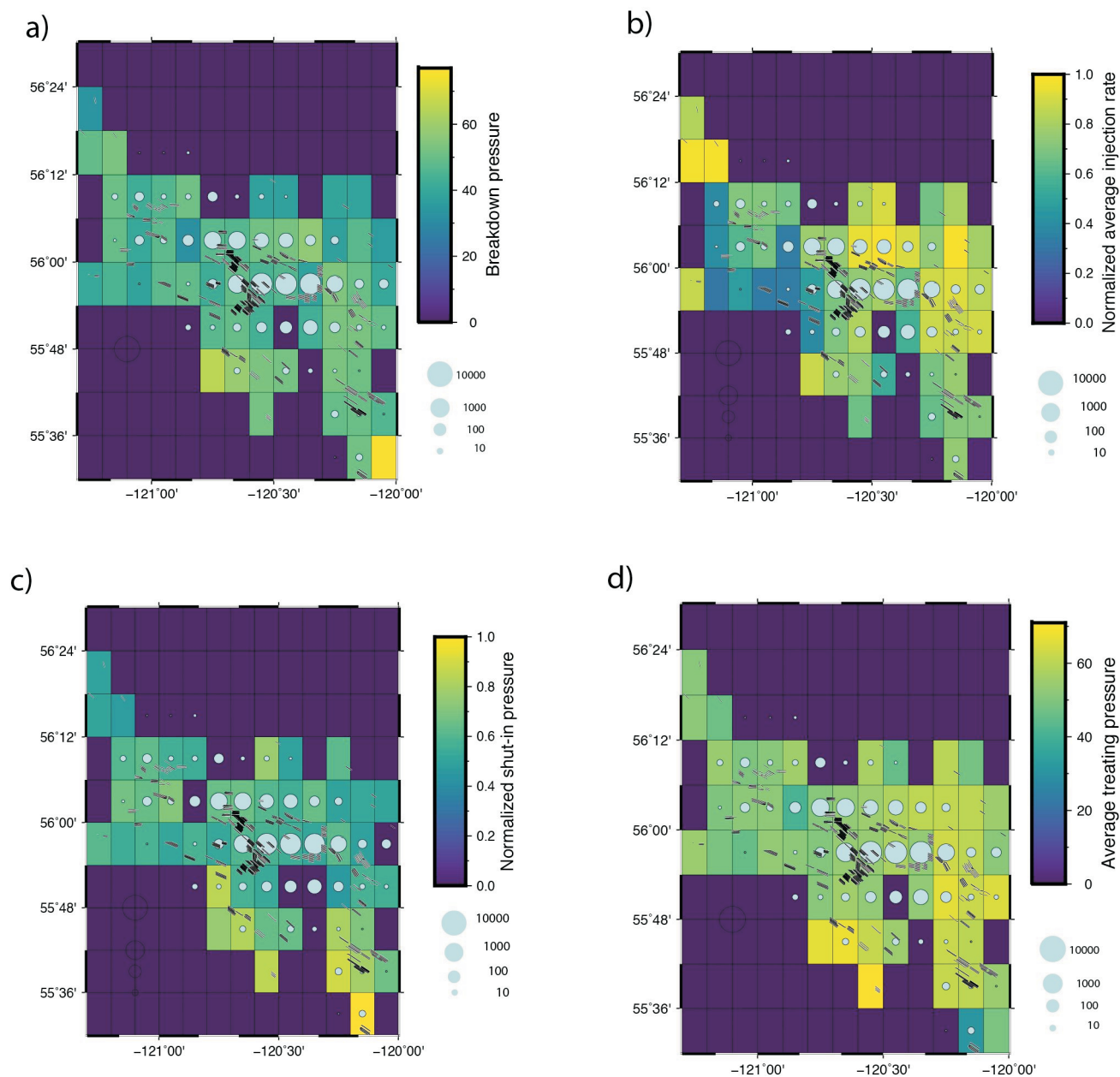


**Figure 6.** The spatiotemporal relationship between hydraulic-fracturing operational parameters and injection-induced earthquakes in the Kiskatinaw Seismic Monitoring and Mitigation Area, northeastern British Columbia. **a)** The background colour in each  $0.1^\circ \times 0.1^\circ$  cell represents the average breakdown pressure normalized by the maximum value within each cell. The size of the circle at the centre of the cells denotes the number of earthquakes in that cell. Diagrams **b)**, **c)** and **d)** are similar to **a)**, showing the average injected rate, average shut-in pressure and average treating pressure, respectively.

brittle failures. This argument is consistent with the pervasive faulting and fracturing/slickenside structures observed within the core samples of the AM (Sanders et al., 2018); it is also compatible with a recently reported upward seismicity-migration pattern from the target member (Peña Castro et al., 2020; Schultz and Wang, 2020). In contrast, the geomechanical rock properties (e.g., higher clay and TOC content) in the UM may favour stable sliding that results in the strain causing the injection-related deformation being released by aseismic slip (Eyre et al., 2019).

## Discussion

The volume of injected fluid has been regarded as one of the key controlling factors in inducing earthquakes within the WCSB. For example, Farahbod et al. (2015) found that in the Horn River Basin of northeastern BC, IIEs were observed only when the monthly HF-injection volume (summed over the entire basin) exceeded the level of  $2.0 \times 10^4 \text{ m}^3$ . Schultz et al. (2018), relying on a greater quantity of data from the Fox Creek area, suggested that the cu-

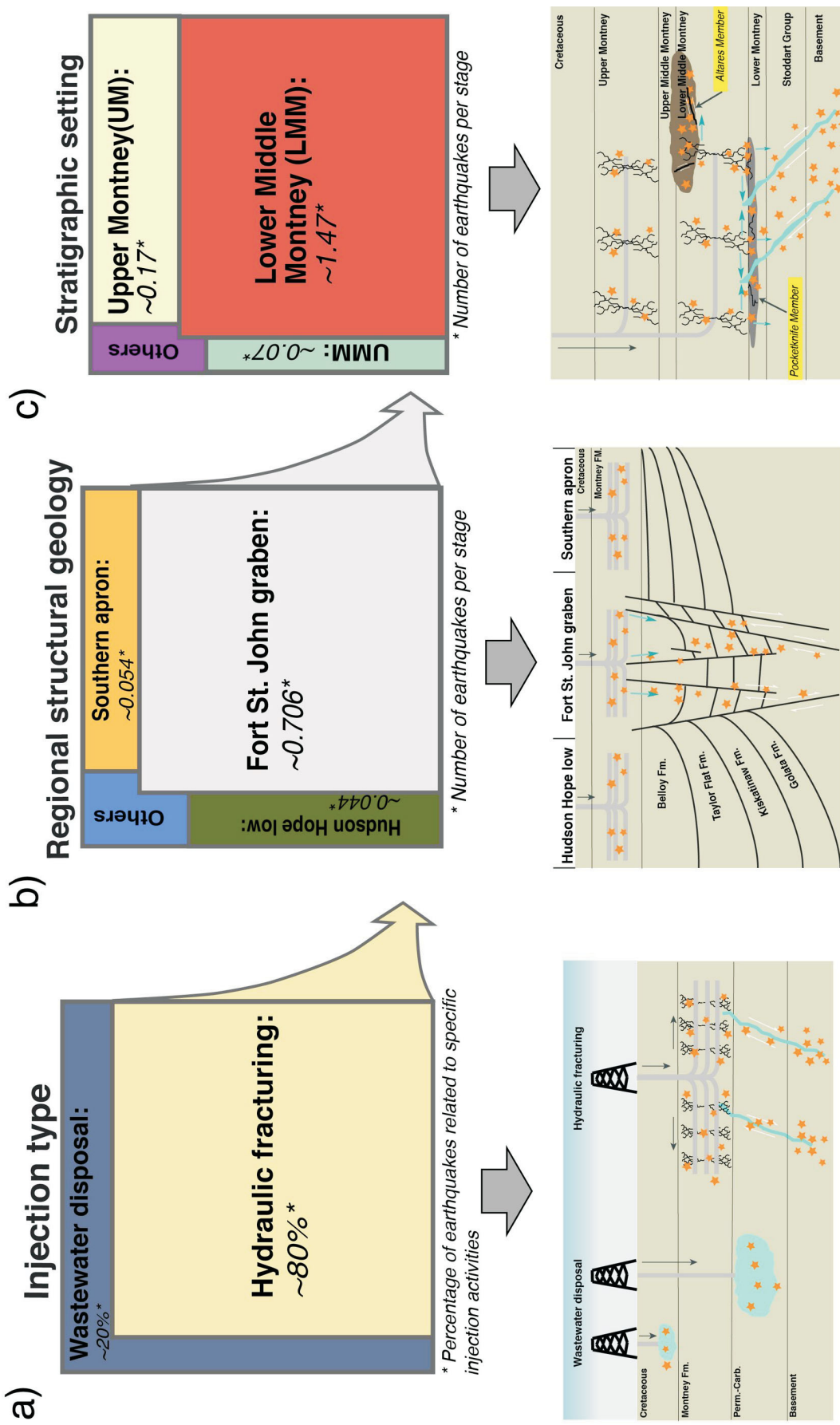


**Figure 7.** Schematic diagram showing the relative significance of physical factors controlling injection-induced earthquakes (IIEs) in the Kiskatinaw Seismic Monitoring and Mitigation Area, northeastern British Columbia. The bottom panels illustrate the corresponding seismogenic mechanisms of IIEs for the top three factors (top panels). **a)** Injection type is the most important factor: approximately 80% of all IIEs (orange stars, given a 3 day and 3 km spatiotemporal correlation-filter criterion) are related to hydraulic fracturing (HF), and can occur in the vicinity of injection depth and the crystalline basement via hydraulic conduits. **b)** Regional structural geology is the second most important factor. The number of earthquakes per HF stage is the highest within the area of the Fort St. John graben filled with subvertical faults (the blue arrows show the potential fluid migration along the graben faults). **c)** Stratigraphic setting is the third important factor: the number of earthquakes per HF stage is the highest when the lower Middle Montney (LMM) is the HF target. The higher IIE rate may be related to the presence of the Altarex and Pocketknife members along the top and bottom sections of the LMM, respectively. Horizontal blue arrows show fluid migration along bedding contacts and possibly intersecting with graben faults, whereas the small vertical blue arrows show the slow diffusion via the permeable Permo-Carboniferous formations below the LMM.

mulative injected volume per each injection pad could be linearly related to the seismicity produced when volumes were approximately  $10^4$ – $10^5$  m<sup>3</sup>. However, observations in the KSMMA study area do not support a linear relationship between the cumulative injected volume and the number of IIEs (Figure 5d). Instead, the FSJG area has a much higher IIE/HF-stage ratio (~0.706) than the two neighbouring areas (0.044 and 0.054; Figure 2b). Since the cumulative injected volume in the FSJG area is also the highest, it is likely that the pervasive fault system in the graben and the large cumulative volume both contribute positively to the higher seismicity.

Based on observations in the study area, it seems that, for the cumulative volume to become an important controlling factor of IIEs, the cumulative injected volume must exceed a certain threshold before the widespread occurrence of IIEs (Figure 5d). Once the outbreak threshold is exceeded, the occurrence rate of IIEs can significantly outpace the rate of volume increase. As more fluid is injected into the rock formations, it could lead to more deformation by the poroelastic effects, pore-pressure diffusion to a broader region as well as additional creep and aseismic slip along pre-existing faults that, in turn, cause additional stress perturbations and earthquakes (Segall and Lu, 2015; Deng et al., 2016, 2020; Goebel et al., 2017; Eyre et al., 2019; Yu et al., 2019; Wang et al., 2021). The nonlinear relationship between the number of IIEs and injected volume probably further points to the important role played by regional/local geological structures.

Although the depth resolution to demonstrate that all IIEs associated with HF targeting the LMM are deeper than those targeting the UM or UMM was not determined, results of the STCF analysis clearly suggest that stimulating the relatively deeper LMM correlates with a higher rate of IIEs (Figure 5b). The relatively porous and permeable formations (Permo-Carboniferous) immediately beneath the Montney Formation (i.e., the Belloy Formation, Stoddart Group and Debolt Formation; Figure 1c) may play an important role. Specifically, these formations contain pervasive pre-existing faults, formed during the Paleozoic subsidence, that can be reactivated by injections to trigger IIEs (Barclay et al., 1990; O'Connell, 1994). They can also act as effective conduits for the fluid and stress perturbation caused by injections that reach the deeper, and presumably more seismogenic, crystalline basement (Skoumal et al., 2018). If the geomechanical perturbation caused by each HF stage is comparable regardless of the targeted formation, the probability of causing IIEs through HF stimulations to the LMM becomes higher due to its close proximity to the deeper Permo-Carboniferous formations and crystalline basement.

The sharp geomechanical rock-property contrast between the LMM and both the AM and PKM may also contribute to

the higher seismogenic potential of the LMM, as the injected fluid can migrate more easily along the bedding contacts to a broader area (Sanders et al., 2018). Such horizontal migration may increase the probability of injected fluid reaching more subvertical faults within the FSJG and potentially triggering more IIEs in the crystalline basement (Figure 7c). The fact that HF stimulations targeting the LMM within the HHL and southern apron areas have caused considerably fewer IIEs than those within the FSJG should be noted. One interpretation could be that the total injected volume within the HHL and southern apron is below the threshold corresponding to the widespread occurrence of IIEs. Meanwhile, the possibility that the interactions between the inferred horizontal migration (due to the bedding contacts) and pervasive subvertical faults within the FSJG help to enhance the seismogenic potential of the LMM cannot be ruled out.

Overall, the highly heterogeneous distribution of IIEs in the KSMMA represents the combined effects of different physical mechanisms. When one factor (e.g., HF stimulation) collaborates with the others (e.g., the geological structure of subvertical or thrust faults [Riazi and Eaton, 2020], the existence of stratigraphic members with distinct geomechanical/hydrological characteristics and proximity to the crystalline basement), the likelihood of IIE occurrence becomes substantially higher (Figure 7).

## Conclusion

The spatiotemporal correlation between injection operations and regional seismicity in the KSMMA was investigated. Findings indicate that ~80% of IIEs are associated with HF stimulations in the area. Conducting Monte Carlo tests using synthetic earthquake catalogues showed that the hypothesis whereby regional seismicity is randomly distributed can be statistically rejected (probability  $<10^{-4}$ ). Additionally, HF stimulations performed in the FSJG area have a much higher probability of inducing earthquakes than those undertaken in the surrounding areas (~0.706 vs. <0.05 event per HF stage). Given the same setting of structural geology and injected volume, the seismogenic response to HF stimulations could vary significantly depending on which formation member is targeted. In the KSMMA, the number of HF stages targeting the LMM is only ~1/5 of that targeting the UM, yet the number of corresponding IIEs is higher (~1.47 vs. ~0.17 event per HF stage).

Based on observations, a comprehensive physical model to interpret the contrasting IIEs is proposed. The enhanced seismogenic potential of HF stimulations targeting the LMM could be explained by at least two reasons. Firstly, the LMM is in proximity to deeper permeable formations and subvertical graben faults that may facilitate the downward migration of injected fluid. The associated stress per-

turbation due to elevated pore pressure could help reactivate pre-existing faults in the basement. Secondly, the geomechanical heterogeneity of two geological units (AM and PKM) along the upper and lower boundaries of the LMM may enhance the seismogenesis of local IIEs. The lower TOC content, higher proportion of recrystallized calcite and sharp hydrogeological contrast to other Montney Formation members probably collectively contribute to the inferred geomechanical heterogeneity.

A key implication of this study is that decisions on the geographic location of injection wells and their targeted formations/members can make a big difference in effectively managing the seismic risk due to IIEs. Therefore, HF stimulations targeting members with a higher IIE-triggering capacity (e.g., the LMM in the FSJG area) should be closely monitored. On the other hand, formations without the characteristic conditions associated with IIEs can probably sustain more HF stimulations and/or larger injected volumes under the same regulatory framework. This aspect should be carefully considered when designing HF stimulations to achieve the optimal balance between stimulation efficiency and seismic safety.

## Acknowledgments

The authors wish to thank A. Babaie Mahani and C. Salas for reviewing this paper. The Natural Resources Canada (NRCan) earthquake catalogue can be downloaded through the NRCan website, the seismic waveforms for NRCan stations are publicly available on the Incorporated Research Institutions for Seismology website (network code 1E and PQ) and the injection-well data can be accessed on the BC Oil and Gas Commission website. The enhanced earthquake catalogue produced using the source-scanning based on navigated automated phase-picking method can be obtained by sending a request to the corresponding author. Support for this study was jointly provided by Geoscience BC, with funding to B. Wang and R. Visser, and the Induced Seismicity Research Project of NRCan, with funding to H. Kao and H. Yu.

## References

- Atkinson, G.M., Eaton, D.W., Ghofrani, H., Walker, D., Cheadle, B., Schultz, R., Shcherbakov, R., Tiampo, K., Gu, J., Harrington, R.M., Liu, Y.J., van der Baan, M. and Kao, H. (2016): Hydraulic fracturing and seismicity in the Western Canada Sedimentary Basin; *Seismological Research Letters*, v. 87, no. 3, p. 631–647, URL <<https://doi.org/10.1785/0220150263>>.
- Babaie Mahani, A. (2021): Seismic *b*-value within the Montney play of northeastern British Columbia, Canada; *Canadian Journal of Earth Sciences*, v. 58, no. 8, p. 720–730, URL <<https://doi.org/10.1139/cjes-2020-0157>>.
- Babaie Mahani, A., Kao, H., Walker, D., Johnson, J. and Salas, C. (2016): Performance evaluation of the regional seismograph network in northeast British Columbia, Canada, for monitoring of induced seismicity; *Seismological Research Letters*, v. 87, no. 3, p. 648–660, URL <<https://doi.org/10.1785/0220150241>>.
- Babaie Mahani, A., Malytskyy, D., Visser, R., Hayes, M., Gaucher, M. and Kao, H. (2020): Well-log-based velocity and density models for the Montney unconventional resource play in northeast British Columbia, Canada, applicable to induced seismicity monitoring and research; *Seismological Research Letters*, v. 92, no. 2A, p. 886–894, URL <<https://doi.org/10.1785/0220200213>>.
- Bao, X. and Eaton, D.W. (2016): Fault activation by hydraulic fracturing in western Canada; *Science*, v. 354, no. 6318, p. 1406–1409, URL <<https://doi.org/10.1126/science.aag2583>>.
- Barclay, J., Krause, F., Campbell, R. and Utting, J. (1990): Dynamic casting and growth faulting: Dawson Creek graben complex, Carboniferous–Permian Peace River embayment, western Canada; *Bulletin of Canadian Petroleum Geology*, v. 38, no. 1, p. 115–145, URL <<https://doi.org/10.35767/gscpgbull.38a.1.115>>.
- BC Oil and Gas Commission (2021): Hydraulic fracture summary data; BC Oil and Gas Commission, URL <<https://www.bcogc.ca/>> [July 2021].
- Davies, G.R., Watson, N., Moslow, T.F. and MacEachern, J.A. (2018): Regional subdivisions, sequences, correlations and facies relationships of the Lower Triassic Montney Formation, west-central Alberta to northeastern British Columbia, Canada—with emphasis on role of paleostructure; *Bulletin of Canadian Petroleum Geology*, v. 66, no. 1, p. 23–92.
- Deng, K., Liu, Y. and Harrington, R. M. (2016): Poroelastic stress triggering of the December 2013 Crooked Lake, Alberta, induced seismicity sequence; *Geophysical Research Letters*, v. 43, no. 16, p. 8482–8491, URL <<https://doi.org/10.1002/2016GL070421>>.
- Deng, K., Liu, Y. and Chen, X. (2020): Correlation between poroelastic stress perturbation and multidisposal wells induced earthquake sequence in Cushing, Oklahoma; *Geophysical Research Letters*, v. 47, no. 20, art. e2020GL089366, URL <<https://doi.org/10.1029/2020GL089366>>.
- Eaton, D.W., Ross, G.M. and Hope, J. (1999): The rise and fall of a cratonic arch: a regional seismic perspective on the Peace River Arch, Alberta; *Bulletin of Canadian Petroleum Geology*, v. 47, no. 4, p. 346–361.
- Ellsworth, W.L. (2013): Injection-induced earthquakes; *Science*, v. 341, no. 6142, art. 1225942, URL <<https://doi.org/10.1126/science.1225942>>.
- Eyre, T.S., Eaton, D.W., Garagash, D.I., Zecevic, M., Venieri, M., Weir, R. and Lawton, D.C. (2019): The role of aseismic slip in hydraulic fracturing-induced seismicity; *Science Advances*, v. 5, no. 8, art. eaav7172, URL <<https://doi.org/10.1126/sciadv.aav7172>>.
- Farahbod, A.M., Kao, H., Walker, D.M., Cassidy, J.F. and Calvert, A. (2015): Investigation of regional seismicity before and after hydraulic fracturing in the Horn River Basin, northeast British Columbia; *Canadian Journal of Earth Sciences*, v. 52, no. 2, p. 112–122.
- Galloway, E., Hauck, T., Corlett, H., Pană, D. and Schultz, R. (2018). Faults and associated karst collapse suggest conduits for fluid flow that influence hydraulic fracturing-induced seismicity; *Proceedings of the National Academy of Sciences*, v. 115, no. 43, p. E10003–E10012, URL <<https://doi.org/10.1073/pnas.1807549115>>.

- Goebel, T., Weingarten, M., Chen, X., Haffener, J. and Brodsky, E. (2017). The 2016  $M_w$  5.1 Fairview, Oklahoma earthquakes: evidence for long-range poroelastic triggering at >40 km from fluid disposal wells; *Earth and Planetary Science Letters*, v. 472, p. 50–61.
- Healy, J.H., Rubey, W.W., Griggs, D.T. and Raleigh, C.B. (1968): The Denver earthquake; *Science*, v. 161, no. 3848, p. 1301–1310, URL <<https://doi.org/10.1126/science.161.3848.1301>>.
- Ikari, M.J., Niemeijer, A.R., Spiers, C.J., Kopf, A.J. and Saffer, D.M. (2013): Experimental evidence linking slip instability with seafloor lithology and topography at the Costa Rica convergent margin; *Geology*, v. 41, no. 8, p. 891–894.
- Kao, H., Visser, R., Smith, B. and Venables, S. (2018): Performance assessment of the induced seismicity traffic light protocol for northeastern British Columbia and western Alberta; *The Leading Edge*, v. 37, no. 2, p. 117–126, URL <<https://doi.org/10.1190/tle37020117.1>>.
- Keranen, K.M. and Weingarten, M. (2018): Induced seismicity; *Annual Review of Earth and Planetary Sciences*, v. 46, no. 1, p. 149–174, URL <<https://doi.org/10.1146/annurev-earth-082517-010054>>.
- Lei, X., Huang, D., Su, J., Jiang, G., Wang, X., Wang, H., Guo, X. and Fu, H. (2017): Fault reactivation and earthquakes with magnitudes of up to  $M_w$  4.7 induced by shale-gas hydraulic fracturing in Sichuan Basin, China; *Scientific Reports*, v. 7, no. 1, 7971, URL <<https://doi.org/10.1038/s41598-017-08557-y>>.
- Lei, X., Wang, Z. and Su, J. (2019): The December 2018  $M_L$  5.7 and January 2019  $M_L$  5.3 earthquakes in south Sichuan basin induced by shale gas hydraulic fracturing; *Seismological Research Letters*, v. 90, no. 3, p. 1099–1110.
- Natural Resources Canada (2021): Search the earthquake database; Natural Resources Canada, URL <<http://www.earthquakescanada.nrcan.gc.ca/stndon/NEDB-BNDS/bulletin-en.php>> [July 2020].
- O’Connell, S.C. (1994): Geological history of the Peace River Arch; *in* Geological Atlas of the Western Canada Sedimentary Basin, G.D. Mossop and I. Shetsen (comp.), Canadian Society of Petroleum Geologists, Calgary, Alberta, and Alberta Research Council, Edmonton, Alberta, p. 431–438.
- Peña Castro, A.F., Roth, M.P., Verdecchia, A., Onwuemeka, J., Liu, Y., Harrington, R.M., Zhang, Y. and Kao, H. (2020): Stress chatter via fluid flow and fault slip in a hydraulic fracturing-induced earthquake sequence in the Montney Formation, British Columbia; *Geophysical Research Letters*, v. 47, no. 14, art. e2020GL087254, URL <<https://doi.org/10.1029/2020GL087254>>.
- Raleigh, C., Healy, J. and Bredehoeft, J. (1976): An experiment in earthquake control at Rangely, Colorado; *Science*, v. 191, no. 4233, p. 1230–1237.
- Riazi, N. and Eaton, D.W. (2020): Anatomy of a buried thrust belt activated during hydraulic fracturing; *Tectonophysics*, v. 795, art. 228640 URL <<https://doi.org/10.1016/j.tecto.2020.228640>>.
- Sanders, S., Etienne, C., Gogolick, A., Kelly, D. and Zonneveld, J.-P. (2018): The Middle Montney Altares Member: lithology, depositional setting and significance for horizontal drilling and completion in the Altares field, British Columbia; *Bulletin of Canadian Petroleum Geology*, v. 66, no. 1, p. 318–337.
- Schultz, R. and Eaton, D.W. (2018): Increased likelihood of induced seismicity in highly overpressured shale formations; *Geophysical Journal International*, v. 214, no. 1, p. 751–757, URL <<https://doi.org/10.1093/gji/ggy167>>.
- Schultz, R. and Wang, R. (2020): Newly emerging cases of hydraulic fracturing induced seismicity in the Duvernay East shale basin: *Tectonophysics*, v. 779, art. 228393, URL <<https://doi.org/10.1016/j.tecto.2020.228393>>.
- Schultz, R., Corlett, H., Haug, K., Kocon, K., MacCormack, K., Stern, V. and Shipman, T. (2016): Linking fossil reefs with earthquakes: geologic insight to where induced seismicity occurs in Alberta; *Geophysical Research Letters*, v. 43, no. 6, p. 2534–2542, URL <<https://doi.org/10.1002/2015GL067514>>.
- Schultz, R., Atkinson, G., Eaton, D., Gu, Y. and Kao, H. (2018): Hydraulic fracturing volume is associated with induced earthquake productivity in the Duvernay play; *Science*, v. 359, no. 6373, p. 304–308.
- Segall, P. and Lu, S. (2015): Injection-induced seismicity: poroelastic and earthquake nucleation effects; *Journal of Geophysical Research: Solid Earth*, v. 120, no. 7, p. 5082–5103, URL <<https://doi.org/10.1002/2015JB012060>>.
- Shen, L.W., Schmitt, D.R. and Haug, K. (2019): Quantitative constraints to the complete state of stress from the combined borehole and focal mechanism inversions: Fox Creek, Alberta; *Tectonophysics*, v. 764, p. 110–123.
- Skoumal, R.J., Brudzinski, M.R. and Currie, B.S. (2018): Proximity of Precambrian basement affects the likelihood of induced seismicity in the Appalachian, Illinois, and Williston Basins, central and eastern United States; *Geosphere*, v. 14, no. 3, p. 1365–1379.
- Tan, F., Kao, H., Nissen, E. and Eaton, D. (2019): Seismicity-scanning based on navigated automatic phase-picking; *Journal of Geophysical Research: Solid Earth*, v. 124, no. 4, p. 3802–3818, URL <<https://doi.org/10.1029/2018JB017050>>.
- Verberne, B., Spiers, C.J., Niemeijer, A.R., De Bresser, J., De Winter, D. and Plümper, O. (2014): Frictional properties and microstructure of calcite-rich fault gouges sheared at sub-seismic sliding velocities; *Pure and Applied Geophysics*, v. 171, no. 10, p. 2617–2640.
- Visser, R., Smith, B., Kao, H., Babaie Mahani, A., Hutchinson, J. and McKay, J. (2017): A comprehensive earthquake catalogue for northeastern British Columbia and western Alberta, 2014–2016; Geological Survey of Canada, Open File 8335, 28 p., URL <<https://doi.org/10.4095/306292>>.
- Visser, R., Kao, H., Smith, B., Goerzen, C., Kontou, B., Dokht, R.M.H., Hutchinson, J., Tan, F. and Babaie Mahani, A. (2020): A comprehensive earthquake catalogue for the Fort St. John–Dawson Creek region, British Columbia, 2017–2018; Geological Survey of Canada, Open File, 8718, 28 p., URL <<https://doi.org/10.4095/326015>>.
- Wang, B., Harrington, R.M., Liu, Y., Kao, H. and Yu, H. (2020): A study on the largest hydraulic-fracturing-induced earthquake in Canada: observations and static stress-drop estimation; *Bulletin of the Seismological Society of America*, v. 110, no. 5, p. 2283–2294, URL <<https://doi.org/10.1785/0120190261>>.
- Wang, B., Verdecchia, A., Kao, H., Harrington, R.M., Liu, Y. and Yu, H. (2021). A study on the largest hydraulic fracturing induced earthquake in Canada: numerical modeling and triggering mechanism; *Bulletin of the Seismological Society of America*, v. 111, no. 3, p. 1392–1404, URL <<https://doi.org/10.1785/0120200251>>.
- Yu, H., Harrington, R.M., Liu, Y. and Wang, B. (2019): Induced seismicity driven by fluid diffusion revealed by a near-field hydraulic stimulation monitoring array in the Montney Basin, British Columbia; *Journal of Geophysical Research:*

- Solid Earth, v. 124, no. 5, p. 4694–4709, URL <<https://doi.org/10.1029/2018JB017039>>.
- Yu, H., Harrington, R.M., Kao, H., Liu, Y., Abercrombie, R.E. and Wang, B. (2020): Well proximity governing stress drop variation and seismic attenuation associated with hydraulic fracturing induced earthquakes; *Journal of Geophysical Research: Solid Earth*, v. 125, no. 9, art. e2020JB020103, URL <<https://doi.org/10.1029/2020JB020103>>.
- Yuan, J., Kao, H. and Yu, J. (2020): Depth-scanning algorithm: accurate, automatic, and efficient determination of focal depths for local and regional earthquakes; *Journal of Geophysical Research: Solid Earth*, v. 125, no. 7, art. e2020JB019430, URL <<https://doi.org/10.1029/2020JB019430>>.
- Zoback, M.D. and Lund Snee, J.-E. (2018): Predicted and observed shear on pre-existing faults during hydraulic fracture stimulation; *in* SEG International Exposition and 88<sup>th</sup> Annual Meeting; Society of Exploration Geophysicists, October 14–19, 2018, Anaheim, California, Technical Program 2018 Expanded Abstracts, p. 3588–3592, URL <<https://doi.org/10.1190/segam2018-2991018.1>>.
- Zonneveld, J.-P. and Moslow, T. F. (2018): Palaeogeographic setting, lithostratigraphy, and sedimentary framework of the Lower Triassic Montney Formation of western Alberta and northeastern British Columbia; *Bulletin of Canadian Petroleum Geology*, v. 66, no. 1, p. 93–127.